AIAA-94-1255-CP

A SMART TELEROBOTIC SYSTEM DRIVEN BY MONOCULAR VISION

R.J.P. deFigueiredo † A. Maccato † P. Wlczek † B. Denney ‡ J. Scheerer ‡

†Dept. of Electrical and Computer Engineering, University of California, Irvine CA 92717
‡McDonnell Douglas Aerospace, 5301 Bolsa Ave, Huntington Beach, CA 92647

Abstract

There is an increasing demand for space robotic systems which can reduce the number of potentially hazardous EVA's on manned space missions. In addition, telerobotic maneuvers can easily become long and tiresome for the operator. This paper describes a robotic system which accepts motion and control commands which can be generated autonomously.

The system developed has been designed to perform an autonomous grapple based on guidance control feedback provided by images from a single camera mounted on the slave robot's end effector. The vision system consists of three parts. The first part is signature based, trained on an arbitrary grapple interface (i.e. no special targets are required for guidance); it provides estimates for the 3D attitude of the interface by interpolating sampled signature correlations. These signatures are essentially the distribution of line orientations obtained by radial integration of the Fourier transform of a pre-processed edge image. The second part estimates the range and bearing of the interface based on the first and second moments of the preprocessed edge image of the interface. And the third stage of the algorithm verifies the results.

The robot path follows a linear translation trajectory which is repeatedly adjusted for errors via the vision system. The end effector's attitude is adjusted along the trajectory such that the grapple interface always remains in center view of the camera.

Introduction

Teleoperations are becoming increasingly important in hazardous environments (e.g. chemical plants, nuclear power plants, space). Space systems applications, such as space-based assembly and maintenance, automatic rendezvous and docking, space exploration, and satellite monitoring and tracking [1] are of particular interest due to potentially long delay times between operator and robot. For instance, it has been estimated that robotic operations can take several times as long as extra-vehicular activity (EVA) to perform similar tasks [2,3]. Long delay times and limited bandwidth require the robot to accept only high level commands and to possess locally a certain degree of autonomy.

Object recognition and attitude determination of objects are essential components for successful sensor based teleoperational semi-autonomous robotic systems. This paper will cover camera based systems, due to the relatively low cost of CCD cameras and their wide use in remote robotic systems.

Current vision based robotic systems utilize visual guidance targets. These targets must be placed on objects with which the robot is to interact[4]. However, when the objects are not readily accessible to humans, which is the case when operating in a hostile environment such as space, the system restricts the class of robotic interactions to those which are specifically identified and designed a priori.

The new vision system developed eliminates the need for these guidance targets by allowing the object, or part of the object (i.e. a grapple fixture), to become the robot's visual guidance target. This is accomplished by teaching the vision system the object by presenting different views. This training could be done with a physical object or by using a CAD model of the object.

The complete description of a particular target relative to the camera consists of six parameters: roll, pitch, yaw, range, and two bearing parameters. All six can be estimated, in principle, from a single camera image and knowledge of the target's solid geometry.

We have developed a new technique for determining the three-dimensional roll, pitch, and yaw attitude target parameters and the three translation parameters assuming that the object is known and unoccluded.

Method

We restrict the class of images to those of machined objects, which characteristically produce sharp edge discontinuities. The edge discontinuities result from the projection onto the image plane of the polytopes, cylinders and conic sections comprising the object. Our approach relies on these projected edges as the basic features required to analyze and interpret the image data.

Attitude Estimation

The technique for estimating the attitude relies on extracting a signature of the object as viewed by the camera, and then matching it against signatures of the same object with known attitudes, generated off line

from a model of that object. The attitude estimate is obtained by interpolating among the signatures with the highest matching scores. The overall procedure is diagramed in Figures 1.

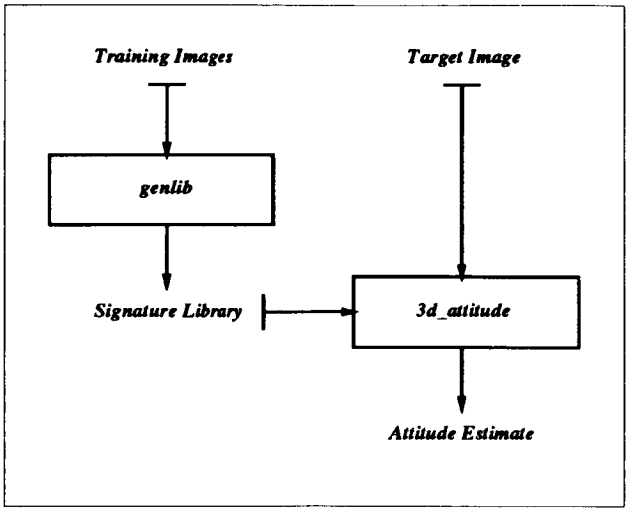

Figure 1: Overall data flow diagram for the estimation of the attitude parameters.

The algorithm computes as a signature the distribution of edge segments in the image as a function of orientation in the image plane. When an object undergoes an attitude transformation, the distribution of line orientations in the image plane changes; therefore, the signature contains implicit information about the object's attitude. On the other hand, the signature is insensitive to the range and bearing of the object, as these do not affect the distribution of line orientations in the image. The signature matching procedure approximates the inverse map from line orientations to object attitude.

The signature extraction computation involves three steps. First, a binary line image is obtained from the original picture (Fig. 2), reducing the effect of changes in illumination of the target (Fig. 3). The preprocessing requests identification of the object within the field of view, and removal of clutter in the image. We achieve this by an image segmentation strategy discussed in detail in the Appendix. The line image is then mapped into the two-dimensional Fourier domain, effectively collapsing range and bearing information, while preserving information on the object's roll, pitch, and yaw (Fig. 4). Lastly, a weighted sum of the magnitude in the Fourier image yields the distribution of line segments as a function of orientation, which serves as an attitude signature (see Gonzales and Wintz[5] for an introductory discussion on the properties of the Fourier Transform applied to image processing)(Fig. 5).

In particular, the Fourier transform provides an efficient and robust means of extracting the signature. In essence, any straight line in the image plane is mapped by the Fourier transformation into a straight line passing through the origin of the transform domain, and orthogonal to the original line. The distance from the origin of the original line results in a complex phase modulation of its transform. By linearity of the Fourier mapping, an image consisting of several straight lines is transformed into a superposition of lines emanating from the origin. Thus, a radial integration of the Fourier transform's magnitude, about the origin of the transform domain, yields the desired signature. To compensate for the finite thickness and length of actual line segments in the image, the Fourier transform is radially weighted, to deemphasize edge thickness.

The attitude parameters are found by performing a cyclic cross-correlation of the target signature with the library signatures and selecting the maximally correlated match. The best signature picked reflects the object pitch and yaw. The offset of that signature match reflects the roll. Since signatures are 180° symmetrical there is a 180° ambiguity in the roll measurement. This ambiguity will be resolved in the match verification process described in Section 2.3.

Position Estimation

The technique for estimating the range and the two bearing parameters of the object relies on the center of gravity x_c, y_c, and the sum of the variances σ_o^2 along the x-axis σ_x^2 and the y-axis σ_y^2 of the object's edge image:

$$\sigma_o^2 = \sigma_x^2 + \sigma_y^2 \tag{1}$$

The range of the object is determined using σ_o^2. It can be shown, that σ_o^2 is invariant to rotation and translation of the image [6-8]. Using a perspective projection, and assuming that the size of the object is small compared to the range, the distance of the object in the actual image, z_0, is given by,

$$z_0 = \frac{f_0 \times \sigma_{\text{ref}} \times z_{\text{ref}}}{f_{\text{ref}} \times \sigma_o} \tag{2}$$

where σ_o is the square root of the variance of the actual image, f_0 is the focal length of the lens used, σ_{ref} is the square root of the variance in the edge image of the matching signature, f_{ref} is the focal length of the lens used in generating the signature library, and z_{ref} is the range of the object used during training.

By knowing the deviation of the center of gravity of the actual edge image against the center of gravity of the edge image of the matched library signature, the two bearing components are determined by:

$$\rho = \tan^{-1}\frac{x_1}{f_0} - \tan^{-1}\frac{x_{\text{ref}}}{f_{\text{ref}}} \tag{3}$$

$$\phi = \tan^{-1}\frac{y_1}{f_0} - \tan^{-1}\frac{y_{\text{ref}}}{f_{\text{ref}}} \tag{4}$$

where (x_1, y_1) and (x_{ref}, y_{ref}) are the center of gravities of the actual edge image and the training edge image respectively. ρ and ϕ are the values of the bearing parameters along the y-axis and x-axis respectively.

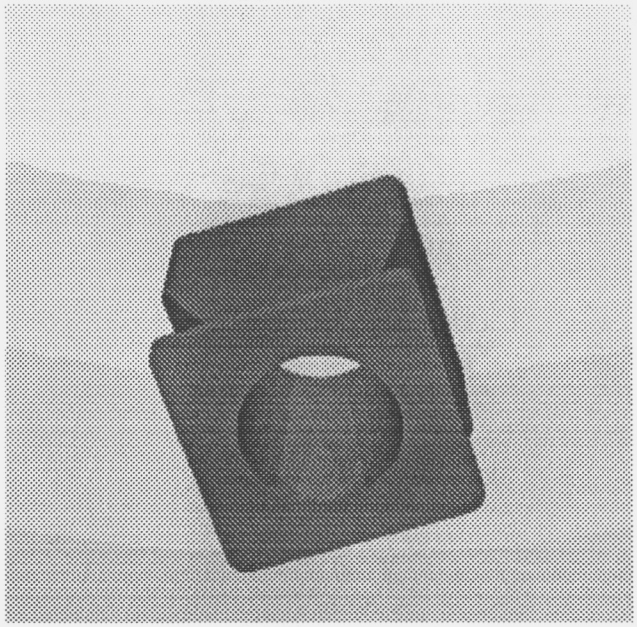

Figure 2: Synthetic image of the Micro Interface device, a typical machined object.

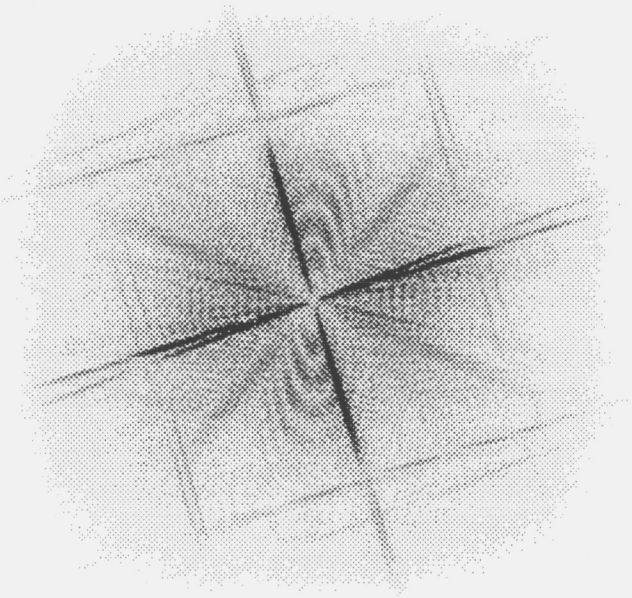

Figure 4: The weighted 2D FFT transform of the edge image of the Micro Interface Device.

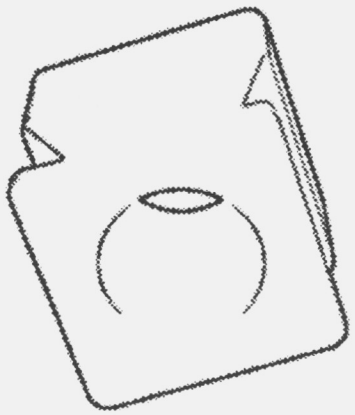

Figure 3: The edge image for the Micro Interface device.

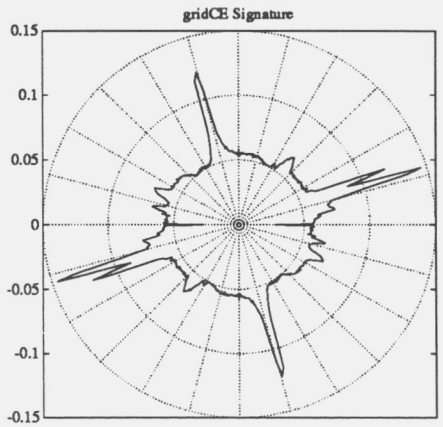

Figure 5: The extracted signature, encoding the distribution of line edge orientations in the original image of the Micro Interface device.

Model Based Attitude Estimation and Verification

The six attitude parameters found in Sections 2.1 and 2.2 must be verified and the ambiguity of the roll must be resolved. This is accomplished with the help of a perspective projection (overlay) of a three-dimensional model of the target (Figure 6) in a cross correlation with the edge image of the object seen by the camera. The overlay with the highest correlation yields the best estimate of the attitude and position of the target.

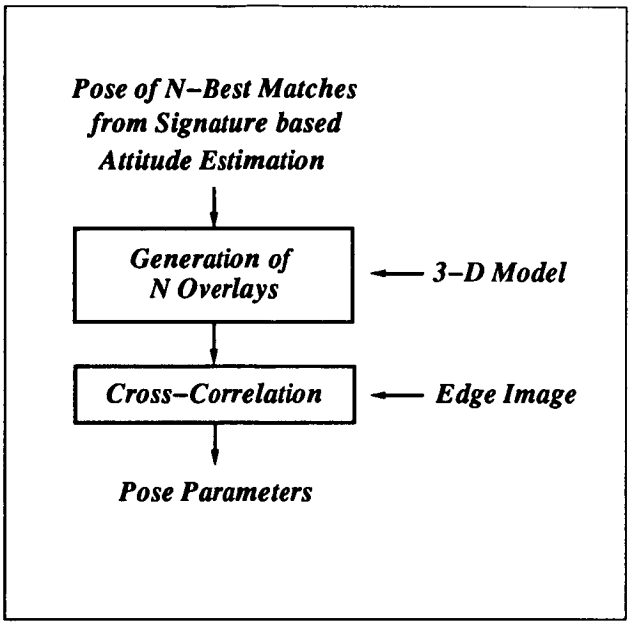

Figure 6: Data flow diagram for estimating the pose of an object based on the projection of a three-dimensional model of the target

The six pose parameters of the n-best matches from the signature based algorithm in Section 2.1 were used to generate n corresponding overlays. A typical overlay is shown in Fig. 7. Those overlays were matched

The three-dimensional model of the object was defined in terms of polygons where each polygon was derived by its vertices. To each polygon a surface normal was assigned to calculate the visibility of the polygon for the current attitude of the object. The visibility check was achieved by determining the sign of the dot product between the normal vector and a vector extending from the the polygon to the view point. For positive values the polygon was visible and for negative values invisible.

To increase the robustness and precision of the cross correlation we correlate the directions of the edges with the direction of the overlay edges. By looking at the directional image gradient we obtain not only the strength of the edge but also its direction. The

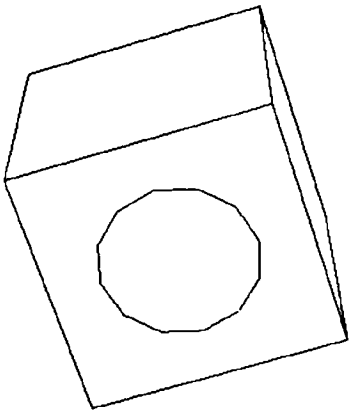

Figure 7: Example of an overlay which was used in a cross correlation to estimate the pose of a target (The jagged edges are caused by the typ-setting process).

modified cross correlation can be stated as

$$match(i,j) = \sum_{x=0}^{N_x} \sum_{y=0}^{N_y} \left| \langle \vec{pt}_{im}\ (x,y)\ \vec{pt}_{ov}\ (i+x, j+y) \rangle \right| \tag{5}$$

where $\langle \cdot \rangle$ denotes the dot product between two vectors. The vectors $\vec{pt}_{im}\ (x,y)$ and $\vec{pt}_{ov}\ (x,y)$ are defined as the two-dimensional vector $[\frac{\partial f(x,y)}{\partial x}, \frac{\partial f(x,y)}{\partial y}]^T$ from the camera image and overlay image respectively. It has to be noted that in Equation 5 we only have to perform the cross correlation in the vicinity of the projection of the object model because the signature based algorithm gives reliable estimates of the position of the target.

The combination of the signature based method shown in Section 2.1 and the above approach based on cross correlation allows us to overcome one of the main disadvantages of the model based methods shown in the literature [9-10] where a correspondence had to be established between image features and model features to solve for the attitude parameters. With the signature based algorithm we are able to prune down the search tree of possible aspects of the model and reduce the range of the cross correlation considerably.

Robot Control

The algorithm for moving the robot towards the target to perform a grapple is described below:

- Using a camera mounted on the end effector, estimate the position and attitude of the target (i.e the handle to be grappled) with respect to the

camera. We will call this frame $\hat{H}$ where the term frame refers to both attitude and position.

- We can define a frame, C_{FH}, with respect to the target, which is the desired final frame of the camera for the approach. Now we can use our estimate for the target to come up with an estimate for C_F, called $\hat{C_F}$, with respect to the Camera frame C. If C is within tolerable limits of C_F then we are at the final position and attitude and can grapple the object.
- If we have not reached C_F then we can calculate our next desired camera position by using the following constraints on the next camera frame, denoted by $N(C)$.
  1. The origin of $N(C)$, denoted by $N(C)_0 = N(C_0)$, falls on the line $\overline{C_0 C_{F0}}$.
  2. $N(C)$ should be at most a distance of $d_{\max}$ from C.
  3. The z-axis of $N(C)$, denoted by $N(C_z)$ should point towards $\hat{H}_0$.
  4. $N(C_x)$ should be perpendicular to both $N(C_z)$ (of course) and $\hat{H}_y$. In particular the sign of the vector is defined by $N(C_x) = \hat{H}_y \times N(C_z)$.
- We can calculate $N(G)$ with respect to G from $N(C)$, since the relationship of the camera frame C to the end effector frame G is known. This information can be put in the form of relative (x, y, z, R, P, Y) moves.
- Command the robot to make the relative move calculated above.
- Repeat the entire process.

Results

We have tested the algorithm on a set of synthetic images of an interface device used in space system applications (Fig. 2). The Micro Interface device is used in SSF robotic operations. A ray-tracer was used to generate the synthetic images' aspect transformations of the target with respect to the image plane. Although the results presented in sections 3.1-3.4 were generated with synthetic images, similar results have been obtained for real camera images.

A 5×5 signature library was generated from synthetic images to cover a square patch 10° on the side in the pitch–yaw plane with an inter-signature separation of 2.5° in each direction. The center orientation was selected to correspond to a typical view of the Micro Interface during a grasping operation. This signature library was representative of more realistic libraries covering a larger range of pitch and yaw parameter values.

Using this signature library, four tests were performed:

1. Random roll, pitch and yaw attitude estimation.
2. Bearing and Range estimation.
3. Range invariance test of roll, pitch and yaw.
4. Bearing invariance test of roll, pitch and yaw.

For consistency with the ray-tracer program, the target's attitude in all four tests was represented using three Euler angles, which measure attitude through a set of three rotations about the z, x, and again z axes, in the camera's frame of reference (the image plane coincides with the xy-plane, and faces the negative z axis). We denote these three rotation angles by α, β, and γ, respectively. The translation components, range and bearing, of the image plane around the x-axis and y-axis were denoted with z, ϕ, and ρ respectively.

The tests provide evidence for the viability of the approach to 3D attitude and position determination. The procedure accurately estimates the position and the three attitude parameters of the object. The algorithm shows invariance to the range and bearing of the target for the estimation of the 3D attitude. These test results are described in the sections 3.1-3.4.

Roll, Pitch, and Yaw Estimation

A random set of 10 target images with three arbitrary Euler angles was used to test the algorithm's ability to correctly determine the target's attitude. The exact and estimated Euler angles are shown in Table 1.

The average error in any one parameter is 0.6°. The maximum error occurred for the α parameter of Image J, a difference of 2.7°. For this image, the wrong library signature was selected in the matching stage. The difference in the γ parameter partially compensates for this error, reducing the combined $\alpha + \gamma$ angular error for this image to only 1.2°.

Bearing and Range Estimation

A set of 4 target images was used to test the accuracy of the procedure for the bearing parameter and a set of 6 target images was used to test the accuracy for the range. The exact and estimated parameters for range and bearing are shown in Table 2 and Table 3. The average error is 2.2cm for the range estimate and 0.1° for the estimate of the bearing.

Range Invariance

A set of 14 target images was used to test the algorithms sensitivity to the target's variation in range. The range of the target in the training images, used to generate the signature library, was 30cm from the image plane. The exact and estimated Euler angles are

Table 1: Attitude estimation test results.

Image	Exact Angles (degrees)			Estimated Angles (degrees)		
	α	β	γ	α	β	γ
A	16.09	22.63	-8.55	16.57	22.15	-9.98
B	15.24	20.46	2.63	15.60	20.33	2.81
C	18.39	23.27	7.69	19.29	22.44	6.19
D	18.40	22.08	-4.55	17.91	21.89	-3.65
E	19.67	23.51	-1.27	20.57	23.11	-1.55
F	16.92	24.55	5.33	16.90	24.36	4.78
G	17.60	23.81	-0.45	17.86	23.51	-0.14
H	19.15	21.31	-5.24	17.95	21.38	-3.51
I	15.17	20.24	-4.50	15.32	20.01	-4.22
J	15.27	23.68	-2.81	12.50	24.74	-0.70

Table 2: Range estimation test results.

Image	Range (cm)	Estimated Range (cm)
A	31	31.17
B	35	35.70
C	39	40.00
D	45	46.30
E	60	62.10
F	90	98.00

Table 3: Bearing estimation test results.

Image	Bearing (degrees)		Estimated Bearing (degrees)	
A	1	0	1.00	0.02
B	2	0	2.00	0.05
C	3	0	3.07	0.13
D	4	0	4.14	0.18

shown in Table 4, for various target ranges. Angles are measured in degrees, range in centimeters.

The errors incurred are moderate, and degrade as the range increases. The maximum error occurred for the α parameter of Image L, a difference of 5.0°. For this image, the wrong library signature was selected in the matching stage. The difference in the γ parameter partially compensates for this error, reducing the combined $\alpha + \gamma$ angular error for this image to only 1.5°.

Table 4: Range invariance test results.

Image	Range (cm)	Exact Euler Angles (degrees)		
		α	β	γ
*	30	17.500	22.500	0.000
Image	Range (cm)	Estimated Euler Angles (degrees)		
		α	β	γ
A	30	17.553	22.342	0.000
B	31	17.455	22.199	0.000
C	32	17.514	22.193	0.000
D	33	17.463	22.116	0.000
E	34	17.467	21.989	0.000
F	35	17.436	21.827	0.000
G	36	17.468	21.533	0.000
H	37	17.492	21.529	0.141
I	38	17.412	21.257	0.141
J	39	17.521	21.351	0.000
K	45	18.068	20.050	0.140
L	60	22.500	17.500	-3.518
M	90	17.989	20.885	0.140
N	150	17.776	21.297	0.140

Bearing Invariance

A set of 5 target images was used to test the algorithm's sensitivity to the target's variation in bearing. The bearing of the target in the training images used to generate the signature library was 0° from the image plane's normal. The exact and estimated Euler angles are shown in Table 5, for various target bearings, away from the image plane's normal, in the direction of the positive y-axis. Both Euler angles and bearings are measured in degrees.

The errors incurred are moderate, with a maximum error in the β parameter of Image E, a difference of only 0.4°. Bearings of more than 4° would have brought the target partially outside the field of view of the camera, and were not tested.

Table 5: Bearing invariance test results.

Image	Bearing (degrees)	Exact Euler Angles (degrees) α	β	γ
*	0.0	17.500	22.500	0.000
Image	Bearing (degrees)	Estimated Euler Angles (degrees) α	β	γ
A	0.0	17.553	22.342	0.000
B	1.0	17.435	22.510	0.000
C	2.0	17.472	22.549	0.000
D	3.0	17.385	22.735	0.000
E	4.0	17.337	22.939	0.000

Verification Method Results

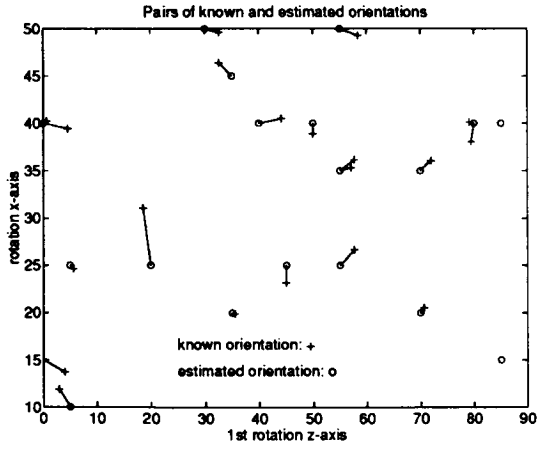

Figure 8: Matching random test points to best overlay candidate (candidates are on a 5 degree spaced grid)

Figure 8 shows the overlay matching results. Each random test point is marked with "+" and has a corresponding (correspondence is indicated by a connecting line) estimate denoted by "o". The estimates in this example fall on a $5° \times 5°$ grid. As seen by the figure, all but one of the matches fell on the nearest grid point (i.e. the estimates were within 5 degrees).

Conclusion

A procedure has been developed to determine the 3D attitude and the position of machined objects without the use of any special marks. Since there is no need for marks, an existing implementation of the algorithm can be quickly adapted to a different object, by supplying a signature library for the new target. Moreover it is not necessary to possess a physical model of the object because it is possible to generate the signature library with a ray-tracer program . In addition the signatures require only 1K bytes of memory each. Thus for a typical signature library of 225 signatures, the signature library is smaller than one 512 by 512 image.

The algorithm relies on standard image processing routines (e.g. edge extraction, 2D Fourier Transformation), which are available in numerous image processing libraries, and fast hardware implementations.

The 2D Fourier Transformation, which is the most time consuming part of the procedure is readily parallelized, so that a real time version of the algorithm can be achieved by distributed hardware.

Although this method was developed under the assumption that there is no clutter in the image and that the target is of a known type, these constraints can be lifted using additional initial scene analysis. For example, the scene can be segmented using standard image processing algorithms, and potential objects can be compared to known objects via signature matching and match verification.

Acknowledgements

This work has been supported in part by McDonnell Douglas Aerospace and the University of California MICRO program.

Appendix

In order to remove background clutter we use information about the constraints of our scene with respect to our target. This appendix discusses in detail the image preprocessing techniques which we used in connection with the robotic grappling application discussed in this paper.

Preprocessing the Raw Image

We start our processing given a single frame 256 gray scale image, I. The image I is filtered three times producing three more useful images. The first is a low pass filtered version of the raw image, denoted by $\tilde{I}$. The next two filtered images are the x and y gradients of the raw image, denoted as $\nabla_x I$ and $\nabla_y I$ respectively. Two binary edge images are then constructed using the above filtered images.

The first edge image is a thin edge image, E, found by,

$$E = \left\{ \left[\frac{\sqrt{(\nabla_x I)^2 + (\nabla_y I)^2}}{(\tilde{I} + 1/2)} \right] > \frac{1}{2} \right\} \qquad (6)$$

where ">" is treated as pixel-wise binary output operator. The above equation attempts to enhance local edge information by dividing the magnitude of the gradient of the raw image by the average neighborhood pixel intensity. Thus small intensity variations in dark regions could be equivalent to larger variations in lighter regions[11].

The second edge image is a thick edge image, E^+, defined as,

$$E^+ = \left\{ \left[\frac{\sqrt{(\nabla_x I)^2 + (\nabla_y I)^2}}{(\tilde{I} + 1/2)} \right] > \frac{1}{4} \right\}. \qquad (7)$$

The image E^+ is nearly identical to E except that the threshold used is lower. Thus, E^+ contains more *white* pixels (pixels which satisfy the binary condition). Therefore, $E \subset E^+$ (i.e. every white pixel of E is a white pixel in E^+). Note that while E provides a cleaner edge image, E^+ preserves the connectivity of the edge image. This connectivity will be used below to determine a processing region which rejects background clutter.

Rejecting Background Clutter

In the discussed application we are interested in finding a handle which is mounted on a predominantly lighter background. In addition we assume that the handle structure will be larger than any unwanted clutter on the same background. Thus, we look for the largest edge structure in a dark region which is contained in a lighter region. This region tells us which information in E should be processed and which information should be rejected. Next we must determine what is light and what is dark as well as what is considered an edge structure.

Using the original raw image, I, we generate a histogram. This gray level histogram is then clustered into three fuzzy classes, *dark pixels*, *medium pixels*, and *light pixels* by using a fuzzy c-means clustering algorithm[12].

The light regions of the raw image are found using the mid-point between the *dark* and *medium pixels* cluster centroids as a image threshold. This thresholded image is then segmented into blobs based on the pixels *8-connectivity*[5,13]. The connectivity analyses only reports significant blobs (blobs which contain a significant number of pixels). Out of all the significant blobs found, the algorithm picks the one with the largest area (number of pixels) as the largest *light* region.

Next, the raw image is thresholded by the mid-point between the *light* and *medium* pixel cluster centroids. This time, all pixels below the threshold are considered logical 1 and all above are logical 0. This new binary image is combined with E^+ using a logical pixel-wise *and*. The resulting binary image contains *edge structure* in the *dark* regions of the raw image.

The *edge structure* is applied to the connectivity analyses algorithm to find all significant connected edge structures in dark regions of the raw image. The resulting processing region is then determined to be the largest *edge structure* in a *dark* region which is within the largest *light* region. If no processing region is found, then the largest *edge structure* in a *dark* region becomes the processing region. And if there where no significant *edge structures* in a dark region found a warning message is issued and the entire image is used as a processing region.

References

[1] R.G.Nornholm, "Space Robotics", *Internal Technical Report MDSSC-SSD*, Report No. MDC 91Q0804-12.

[2] *MDSSC-SSD Maintainability Input for CCO-108 (SS Robotic Costing Proposal)*, Contract NAS 9-18200, December 1992.

[3] W.F. Fisher and C.R. Price, *"Space Station Freedom External Maintenance Task Team"*, Final Report, NASA Johnson Space Center, July 1990.

[4] D.H.Kite and M.Magee, "Determining the 3D Position and Orientation of a Robot Camera using 2D Monocular Vision", *Pattern Recognition*, Vol. 23, No. 8, pp. 819-831, 1990.

[5] R.C.Gonzalez and P.Wintz, *Digital Image Processing*, 2nd ed., Addison Wesley, 1987.

[6] R.Y.Wong and E.L.Hall, "Scene Matching with Invariant Moments", *Computer Graphics and Image Processing*, Vol. 8, pp. 16-24, 1978.

[7] M-K Hu, "Visual Pattern Recognition by Moment Invariants", *IRE Transaction on Information Theory*, Vol. IT-8, pp. 179-187, 1962.

[8] Vishal Markandey and Rui J.P. deFigueiredo, "Robot Sensing Techniques Based on High-Dimensional Moment Invariants and Tensors", *IEEE Transactions on Robotics and Automation*, Vol. 8, pp. 186-195, April 1992.

[9] Y. Kuno, Y. Okamoto and S. Okada, "Robot Vision Using a Feature Search Strategy Generated from a 3-D Object Model", *IEEE Transactions on Pattern Analysis and Machine Intelligence*, Vol. 13, No. 10, 1991.

[10] D. G. Lowe, "Fitting Parameterized Three-Dimensional Models to Images", *IEEE Transactions on Pattern Analysis and Machine Intelligence*, Vol. 13, No. 5, 1991.

[11] R. P. Johnson, "Contrast Based Edge Detection",*Pattern Recognition*, Vol. 23, No. 3/4,, pp. 311-318, 1990.

[12] J. C. Bezdek, *Pattern Recognition with Fuzzy Objective Function Algorithms*, Plenum Press, New York, 1981.

[13] B. K. P. Horn, *Robot Vision*, The MIT Press, Cambridge, Massachusetts, 1986.